Apr 1st, 8:00 AM

Deorbit Maneuver and Targeting Strategy for Unmanned Mars Landers

W. J. Pragluski
Martin Marietta Corporation

D. Marquet

DEORBIT MANEUVER AND TARGETING STRATEGY FOR UNMANNED MARS LANDERS

by

W. J. Pragluski, D. Marquet
Martin Marietta Corporation, Denver, Colorado

SUMMARY

Several deorbit maneuver strategies for unmanned Mars soft landers are evaluated in terms of propulsive efficiency, targeting capability, communication link geometry, and sensitivity to system uncertainties. These strategies include (1) minimum deorbit impulse, (2) minimum entry condition uncertainties, (3) minimum variation in the lander antenna aspect angle during entry, (4) minimum communication range from the lander to the orbiting spacecraft during entry. The selected maneuver strategy is a combination of the above which restricts orbiter lead angles to the range between 0 deg and -10 deg. The analysis covers a range of elliptical orbits with periapsis altitudes of 500 to 2500 KM and apoapsis altitudes of 10,000 to 20,000 KM. The nominal orbit which is selected in order to best satisfy all mission considerations is 1300 KM by 12,500 KM ($h_p \times h_A$).

Mission considerations include orbit orientation of the orbiting spacecraft for planet surface mapping, landing site location between 15 to 30 degrees from the terminator for entry TV imaging, and orbit characteristics which insure a 50-year orbit lifetime and non-occultation of either the Sun or Star Canopus for 30 days after encounter. These constraints, coupled with the uncertainties introduced by trans-Mars navigation uncertainty and orbit insertion maneuver uncertainties, are used in the definition of minimum targeting flexibility required to land at a preselected location (latitude and longitude) and the regions of Mars which can be selected for landing. The selection of a landing site after surveillance from orbit where as much targeting flexibility as possible is desired is also considered.

Two aspects of the error analysis are considered. The first deals with the range of orbits relative to a preselected nominal which might be experienced. The sources leading to this range uncertainty include cruise navigation, orbit insertion maneuver, and orbit trim maneuver. The deorbit maneuver strategy must be capable of compensating for these orbit uncertainties if a preselected landing site is to be acquired.

The second aspect of the error analysis deals with the flight conditions at entry and landing site acquisition accuracy. The uncertainty sources considered here include orbit ephemeris determination accuracy, deorbit maneuver, and atmosphere uncertainties. This aspect of the error analysis leads to the definition of an entry corridor and selection of potential landing areas for early missions.

The final aspect of the analysis includes the effect of targeting flexibility on the post landing communication link characteristics between the lander and orbiting spacecraft. The influence of both aspects of the error analysis on the post landing communication link is discussed.

INTRODUCTION

The analysis of deorbit maneuver strategy can only be meaningful if it is made within the boundaries imposed by scientific objectives of the mission, system capabilities, and constraints imposed on the mission profile by subsystem design considerations. To establish a deorbit maneuver strategy all of the flight operations in the vicinity of Mars must be considered including orbit selection, deorbit impulse size, guidance subsystem accuracies, communication subsystem link geometries, and last, but hardly least, the ability to place the lander at scientifically interesting landing areas. The analysis presented below touches on many of the more important aspects which must be considered. It includes propulsion subsystem considerations for orbit insertion, orbit trim, and deorbit, the error analysis associated with these maneuvers, targeting capability, and communication subsystem link geometry characteristics. These analyses lead to the selection of a deorbit maneuver strategy and range of suggested orbits.

Before proceeding with the analysis, a brief description of the total mission profile is presented below to provide the proper perspective. This includes the more important mission constraints assumed in this analysis. Only the operations in the vicinity of Mars are presented in any detail.

MISSION PROFILE AND CONSTRAINTS

Total Mission Profile

The mission profile considered is shown in Figure 1. The planetary vehicle, orbiting spacecraft and lander, is injected onto a trans-Mars trajectory from an Earth parking orbit. A Sun-Canopus attitude control system is employed during

the cruise mode. At least two midcourse maneuvers might be required during the trip of about 200 days duration. Based on Earth tracking and the desired landing site, the orbit insertion command is calculated and sent to the planetary vehicle. At a programmed time the orbit insertion maneuver is executed. At least four orbits are assumed to determine the ephemeris of the resulting orbit from Earth-based tracking. An orbit trim maneuver may be required to compensate for the off-nominal orbit resulting from approach and orbit uncertainties. Potential landing sites may be viewed from orbit and a site selected. Four to five days after orbit insertion, depending on the desired landing site longitude, the lander is separated from the orbiting spacecraft. The lander orients itself for deorbit firing during a half-hour coast phase required to separate the two vehicles by at least 300 meters. The deorbit engine is fired and the lander then coasts to the desired atmospheric entry point. Between deorbit firing and entry the lander is reoriented to provide a nominal entry angle of attack of zero degrees. A ballistic entry is followed by parachute deployment at an altitude of about 18,000 ft above the surface. Vernier ignition and parachute jettison occur at an altitude of about 5000 ft. Vernier shutdown occurs 10 feet above the surface and the lander free-falls to the surface. The details of the terminal phase system are discussed in another paper and are not considered here.

Representative Launch Window

The 1973 Mars mission is selected here as a representative opportunity to discuss some of the orbit insertion and orbit geometry considerations. The energy contours for a Type I mission are presented in Figure 2. The relationship between Earth departure energy, C_3, and Mars approach energy, V_{HE}, is illustrated. Two constraint boundaries are also shown. The lower limit on encounter date is established by limiting the V_{HE} to less than 3.25 KM/SEC. The declination of the departure asymptote, δ_{HE_∞}, has been constrained to be less than 35 deg from a range safety consideration. The cross hatched region is where the most favorable payload margins occur. This is the combination of C_3 and V_{HE} which results in near maximum payloads in orbit about Mars. Three circled points of interest are shown. Points (1) and (2) are used for the discussion of periapsis shift requirements presented below. Point (3) is used for the example of occultation constraints.

Primary Mission Constraints

The mission constraints considered in this paper are given in Table I below, along with a brief comment on their source and influence on the mission.

NEAR MARS PROPULSIVE PHASES

Orbit Insertion Phase

The orbit insertion phase is discussed in terms of the impulse required and the associated errors. Only insertion at the periapsis of the approach hyperbola is discussed in this section. The influ-

TABLE I
MISSION CONSTRAINTS

	CONSTRAINT	SOURCE	INFLUENCE
1.	Orbit lifetime of at least 50 years	Non-sterilization of the orbiting spacecraft	Size of orbits
2.	Orbit insertion ΔV_{OI} less than 1.75 KM/SEC	Reasonable weights in orbit	Size of orbits and periapsis shifts allowable
3.	Inclination of orbit to Martian equator greater than 30 deg	Orbiting spacecraft mapping mission	Allowable landing site latitudes
4.	Non-occultation of either the Sun or Canopus for 30 days after encounter	Orbiting spacecraft attitude control reference and power source	Allowable inclinations at Mars
5.	Landing site located between 15 to 30 deg from the terminator	Entry TV imaging	Allowable range of targeting parameter
6.	Orbiter sub-periapsis between zero to 45 deg from the terminator	Orbiter TV imaging	Allowable range of targeting parameter and periapsis shift
7.	Orbit insertion in view of Goldstone	Mission operations	Time of arrival; orbit orientation
8.	$\Delta V_D < 600$ M/SEC	Reasonable lander weights	Allowable range of targeting parameter
9.	$V_{HE} < 3.25$ KM/SEC	Reasonable weights in orbit	Allowable range of orbits and periapsis shift

ence of periapsis shift requirements on $\Delta V_{O.I.}$ is discussed later. Impulsive maneuvers are assumed.

Orbit Insertion Impulse. The maximum $\Delta V_{O.I.}$ considered is 1.75 KM/SEC (Table I). The allowable range of possible orbits with this impulse is shown in Fig. 3 as a function of V_{HE}. For a V_{HE} of 3.25 KM/SEC the apoapsis altitude range is restricted to periapsis altitudes above 1750 KM. In order to consider a 2500 x 10,000 KM orbit the V_{HE} must be less than 3.12 KM/SEC. A conservative 50-year orbit lifetime boundary is also shown.

Orbit Deviation from Nominal

The planned mission will have a preselected landing site and nominal orbit prior to Earth departure. Deviations to this nominal orbit will occur as a result of cruise navigation uncertainty, orbit insertion maneuver uncertainties, and orbit trim maneuver uncertainties. The deorbit maneuver must be capable of compensating for these deviations.

The cruise navigation uncertainty becomes a factor at two times. The first is at the time of the last midcourse correction where navigation uncertainty can lead to a periapsis altitude error of 500 KM (3σ). The second time is a few hours before encounter when the orbit insertion command is calculated and transmitted to the spacecraft. Here the navigation uncertainty is less (300 KM periapsis altitude uncertainty, 3σ) and some of the approach trajectory error resulting from the last midcourse correction can be compensated for. The remaining uncertainties are reflected in orbit errors.

The orbit insertion maneuver is based on the best estimate of the approach trajectory at the time of its calculation and transmittal to the spacecraft. The philosophy used is to accept deviations from the nominal periapsis altitude and adjust the orbital period to give the correct landing site longitude. The nominal periapsis altitude could be regained but an undesirable shift in periapsis location would occur. Navigation uncertainties at that time can result in application of the maneuver at the wrong time and place. In addition, maneuver errors will also be evident. Those assumed here are impulse errors of 5% normal and 3% parallel to the nominal ΔV vector (3σ). The combined effect of these error sources for a mean orbit (1000 x 15,000 KM) is summarized in Table II. This includes a one sigma error in orbit periapsis location, θ_p, of 2.02 deg and an orbital period error of .66 hours. The orbit periapsis altitude can be in error by as much as 500 KM (3σ). These uncertainties tend to get larger as the nominal orbit eccentricity is larger.

The period errors can be compensated for by an orbit trim maneuver made after the orbit ephemeris is established with Earth-based tracking. A maximum maneuver impulse of 150 mps is assumed here with maneuver uncertainties of 5% of impulse (3σ) both normal and parallel to the nominal ΔV. The period error after trim will be .081 hours (one sigma) for the 1000 x 15,000 KM orbit used as an example above. This results in a longitude deviation from desired of 1.18 degrees (one sigma) per orbit. The significance of these deviations in terms of deorbit maneuver strategy requirements is presented later in this analysis.

Deorbit Phase

The deorbit phase is discussed in terms of the impulses required and the associated errors. The Martian entry corridor is also discussed in terms of its influence on the range of entry flight path angles. Figure 4 illustrates the general deorbit geometry. The entry point location, top of the atmosphere, is measured with respect to orbiter periapsis by the angle β, measured positively opposite the direction of motion of the orbiter. The angle β is used as a targeting parameter rather than the actual landing site due to the variation in downrange angle traversed during entry caused by entry flight path angle dispersions and atmosphere uncertainty. The downrange angle, $\Delta\theta$, is between 15 deg and 25 deg.

An important parameter for the analysis of the relay communication link between the lander and the orbiting spacecraft is the orbiter lead angle λ. If the orbiting spacecraft leads the lander at the time of entry, λ is positive.

Deorbit Impulse. The deorbit impulse required as a function of targeting parameter, β, is shown in Fig. 5 for the range of orbits being considered. The solid curves are for the minimum ΔV_D. On these curves the λ becomes more negative with increasing β. The higher the eccentricity of the orbit, low h_p and high h_a, the lower the absolute minimum ΔV_D but the variation of ΔV_D with β is greater than for less eccentric orbits. The ΔV_D required to keep the orbiter lead angle constant at the values 0 deg and -10 deg is also shown. Elevation cutoffs are shown on the minimum ΔV_D curve. This is where the elevation angle of the orbiter above the lander's local horizontal at the time of entry is zero deg (large negative λ). The maximum ΔV_D considered is 600 M/SEC. This restricts the allowable range of β as a function of orbit size and shape and design λ.

Deorbit Error Analysis. Three sources of error exist at the deorbit point which are propagated to a fixed entry altitude. They are then propagated through the unknown atmosphere to yield landing site acquisition accuracies. The three sources of error are (1) navigation uncertainty at the time of deorbit (2) lander orientation at deorbit motor firing, and (3) deorbit motor delivered impulse (cutoff accuracy). Error source (1) is expressed in terms of a covariance matrix of position and velocity errors at the time of deorbit. The standard deviations used

TABLE II

ORBIT INSERTION ERROR SUMMARY

Error Source	Magnitude (3σ)	σ_{θ_p} (Deg)	σ_{t_p} (Hrs)
Navigation uncertainty at last maneuver	500 KM in h_p	.65	-
Navigation uncertainty at insertion calc.	300 KM in h_p	1.69	.42
Misapplication of $\Delta V_{O.I.}$	3% parallel; 5% normal	.89	.52
Combined RSS		2.02 Deg	.66 Hrs

TABLE III

DEORBIT ERROR SUMMARY

Error Source	Magnitude (1σ)	$\sigma\gamma_A$ (Deg)	σ_{DR} (KM)	σ_{DR} (Deg)
(1) Navigation Uncertainty	$x = 18$ KM $\dot{x} = .6$ M/SEC			
	$y = 19$ KM $\dot{y} = 3.3$ M/SEC	.19	38.2 (at entry altitude)	.60
	$z = 12$ KM $\dot{z} = 2.8$ M/SEC			
(2) Pointing	.5 deg	.30	40.6	.64
(3) Impulse	.333%	.20	24.2	.38
(4) A_σ, μ_σ	$\sigma_{R_\sigma} = 5$ KM	.12	-	-
	$\sigma_{\mu_\sigma} = 166$ KM^3/SEC^2			
Total RSS Errors at Entry		..425	60.8	.96
(5) Atmosphere Uncertainty	VM-8 and VM-9	-	94.5 (on surface)	1.6
Landing Site Error		-	110.	1.87

are shown in the summary Table III. The errors at entry due to these three sources can be expressed in terms of errors in entry flight path angle, downrange angle (β), entry velocity, time of entry, and crossrange angle. The errors in γ_A and β are the most important for mission planning purposes.

A maneuver pointing uncertainty of 0.5 deg (1σ) is assumed. The resulting entry flight path angle uncertainty is shown in Fig. 6. A 1300 x 10,000 and 1500 x 20,000 KM are shown. The variation with h_A is more significant than the variation with h_p. Lower θ_p retains the shape of the curves but shifts them to lower ΔV_D. The true anomaly of deorbit, θ_D, is increasing along the curves as shown. The ΔV_D required to give an error in γ_A of zero is very near the minimum ΔV_D for the β range considered. Generally the entry γ_A dispersion can be kept below .30 deg (1σ). Although this error can be kept small, the importance of maintaining a near minimum ΔV_D as part of the deorbit maneuver strategy is clearly evident from the nature of the curves shown in Fig. 6.

The error in γ_A due to source (3) is shown in Fig. 7 for the same two orbits. The variation with ΔV_D is smaller and the magnitude of the $\sigma\gamma_A$ is smaller, less than .20 degrees in all cases. The magnitude of (3) was taken to be .333% (1σ). Source (1) results in a $\sigma\gamma_A$ of about .19 deg. A summary of these errors and also the downrange errors is given in Table III. The effect on γ_A of uncertainty in the Martian radius and gravitational parameter is given. Also shown is the resulting error in landing site location due to propagation of the errors at entry through the unknown atmosphere. The 1σ error is 110 KM.

Entry Corridor. The entry corridor, as defined here, is the relationship between the entry velocity and entry flight path angle which might be experienced as a result of the above uncertainties. As a generalization, it is desirable to enter the light Martian atmosphere with as shallow an entry flight path angle as possible. This results in more time in the atmosphere for the entry vehicle to dissipate the entry velocity energy. The minimum criteria used here to define the entry corridor is to target for an entry flight path angle at least 5 σ of the entry flight path angle uncertainty steeper than a conservative skipout boundary. This insures that the entry is at least 2 σ above the skipout boundary. Table III shows that the 2 σ error in γ_A at entry is .85 deg. The combination of γ_A and V_A which give the same conditions at the beginning of the terminal phase were found to be almost parallel to the skipout boundary, slightly lower slope. The nominal aim line is taken to be 3 σ above this curve. A reasonable range of entry velocities for all orbits considered is 4.0 to 4.5 KM/SEC, 13,100 to 14,750 ft/sec. Considering the possible 3 σ dispersions, the resulting minimum and maximum γ_A are -11.6 and -16.6 deg respectively.

For the first mission to Mars it may be desirable to use a higher nominal aim line to allow for higher navigation uncertainties at the time of deorbit. A recommended maximum boundary is shown in Fig. 8 where a γ_A of -20 deg is the upper limit. Higher γ_A are attractive for several reasons: (1) landing site location accuracy increased; (2) total heating during entry decreased; (3) atmospheric determination accuracy increased. The landed payload becomes very sensitive to γ_A for γ_A steeper than about -20 deg. The shallow entry corridor is used throughout the following analysis.

Figures 5, 6 and 7 of the deorbit phase section are based on the shallow nominal aim line. The effect of γ_A on the minimum deorbit impulse is shown in Fig. 9 for a 1500 x 10,000 KM orbit. The trends shown are similar for the range of orbits considered. The targeting parameter for minimum ΔV_D increases by 12 deg, as γ_A increases from -12 deg to -16 deg. Higher values of β are associated with steeper γ_A.

Targeting Parameter Limits

The targeting parameter, β , limits are a function of orbit size and design maximum ΔV_D. The limits are shown in Fig. 10 for orbiter lead angles constrained between -10 and 0 deg and for maximum ΔV_D of 300 and 600 M/SEC. The ΔV_D is not a constant but varies with β . Also shown are lines of constant coast time, the time from deorbit to entry. This parameter is important in the design of the attitude control system required for the lander during coast and of the battery size required for internal power. An apoapsis altitude of 20,000 KM requires coast times up to 12 hrs for β above 40 deg.

LANDING SITE ACCESSIBILITY

Possible Landing Areas

The possible landing sites are dependent upon the launch window chosen and the mission constraints. Figures 11(a) and 11(b) show the arrival geometry for a launch and arrival date corresponding to points (1) and (2) of Fig. 2. For the early arrival (1), the hyperbolic excess velocity vector is just beneath the Martian equator, 4 deg. All orbits about Mars must include this vector. Any inclination orbit is possible, above 4 deg. Three of the possible orbits are shown, inclinations of -60 deg from the south, -30° from the south, and 30 deg from the north. The orbits shown are posigrade, that is they have a component of their motion in the same direction as the rotation of Mars about its own axis. The direction to the Sun and the Earth are shown as well as the terminator. The locus of natural periapsis is about 60 deg back from the $\vec{V}_{HE}$. The required landing region is constrained to be between 15 deg and 30 deg from the terminator in the sunlight. Only landing sites near the evening terminator are shown for clarity. With no other constraints imposed, almost any latitude on Mars may be reached. Longitude control is possible by adjusting the time of day of encounter or the number of orbits waited before deorbit.

Periapsis Shift Requirements

Another constraint to be placed on the possible landing area is due to the range of targeting parameter, β , given in Fig. 10. A β of 25 deg is chosen as a nominal and a downrange angle during entry, $\Delta\phi$, of 20 deg is taken as representative. If the orbiter periapsis is at natural periapsis only a small area of the possible landing zone can be reached and only a small range of inclinations are allowable. This can be seen by looking at the locus of orbiter periapsis locations required to land 22.5 deg from the terminator with a β of 25 deg. In order to extend the range of allowable inclinations and thus landing site latitudes, periapsis shifts are considered.

The required periapsis shifts as a function of orbit inclination to land 22.5 deg from the terminator are shown in Fig. 12. Landings near both the evening and morning terminator are shown. Only posigrade orbits have been shown since the required $\Delta\omega$ is less than for retrograde orbits. Posigrade orbits also infer non-occultation of the Earth at insertion. The relative ground speed from the orbiting spacecraft is less and relative velocities of entry are less for posigrade orbits. The required $\Delta\omega$ to land near the evening terminator is small, ± 30 deg depending on inclination and arrival date. The required $\Delta\omega$ to land near the morning terminator is large, -80 to 150 deg.

The implication of required $\Delta\omega$ on orbit size is shown in Fig. 13. The boundaries were constructed

assuming a maximum $\Delta V_{O.I.}$ of 1.75 KM/SEC applied tangentially to the approach hyperbola. Positive $\Delta\omega_{REQ}$ require insertion before natural periapsis while negative $\Delta\omega_{REQ}$ require insertion after. For a late arrival date and evening terminator landing site, there is no restriction on the nominal range of orbits. For an early arrival date there is some restriction on the less eccentric orbits but an inclination of -20°, $\Delta\omega_{REQ}$ of zero deg, eliminates only a small corner of the nominal range. For landing sites near the morning terminator an inclination of -60 deg has been shown which corresponds to a $\Delta\omega_{REQ}$ of -80 deg for a late arrival. This $\Delta\omega_{REQ}$ is less than -80 deg for inclinations higher than -60 deg. These inclinations are not shown however due to the occultation restrictions discussed in the following section. Morning terminator landing sites are possible however if larger β are employed or the lighting constraint at touchdown is relaxed. Increasing β by 10 deg reduces the $\Delta\omega_{REQ}$ by 10 deg. For a given β allowing the landing site to be 40 deg rather than 30 deg from the terminator reduces the $\Delta\omega_{REQ}$ by 10 deg.

Significance of Occultation Constraints

An important mission constraint is the non-occultation of either the Sun or Canopus for at least 30 days after encounter. The resulting constraint on orbiter inclinations is shown in Fig. 14 as a function of periapsis shift, $\Delta\omega$. A middle arrival date corresponding to point (2) of Fig. 2 is shown. For low periapsis altitude, 500 KM, only posigrade orbits from the south with inclinations between about -20 deg and -70 deg are possible depending upon $\Delta\omega$. For $\Delta\omega$ less than -45 deg, inclinations must be below -60 deg. A higher periapsis altitude extends the possible range of inclinations and $\Delta\omega$. A small range of PN inclinations exist for an h_p of 1500 KM, between about 20 deg and 40 deg. Thus a small landing region in the northern hemisphere is possible for the higher h_p. The variation of the occultation contours is slight for the range of arrival dates considered. The variation with h_A is much less than with h_p.

Landing Area Summary

The shaded areas in Fig. 11(a) and 11(b) show the allowable landing regions for all h_p considered, 500 KM to 2500 KM. Inclinations less than 30 deg are eliminated due to the orbiter mapping constraint. The landing site latitudes lie generally between -30 deg and -60 deg. For a given orbiter inclination the variation in landing site latitude with targeting parameter is small. The higher the inclination the larger the variation in landing site latitude with β.

DEORBIT MANEUVER STRATEGY

Strategies Considered

The following five deorbit maneuver strategies have been considered: (1) minimum deorbit impulse; (2) minimum entry condition uncertainties; (3) minimum variation in the lander aspect angle during entry; (4) minimum communication range from the lander to the orbiting spacecraft during entry; (5) minimum fading margin communication losses during entry. The implications of each strategy are discussed separately and then a reference maneuver strategy is selected.

Minimum ΔV Strategy (#1). The minimum ΔV_D was shown as a function of targeting parameter in Fig. 5 for the range of orbits considered. The orbiter lead angle, λ, becomes more negative with increasing β. For a given β the λ is more negative the less eccentric the orbit ($high_p$ and low_a). Large negative λ, greater than -25°, are undesirable due to the higher communication ranges at the time of entry and the large capsule aspect angles at the beginning of the terminal phase of entry. For this reason high β are undesirable using minimum ΔV_D. For example, for a 1500 x 10,000 KM orbit the λ is more negative than -25 deg for any β above 30 deg. The lead angle is -47 deg at a β of 40 deg. The desire to use larger β than 30 deg to increase the targeting capability led to the search for other higher ΔV_D strategies.

Minimum Entry Condition Uncertainties (#2). The largest error source for entry flight path angle dispersions is orientation as seen in Table III. The variation of the dispersion in entry flight path angle, γ_A, was shown in Fig. 6 as a function of ΔV_D. It was shown that the required ΔV_D to make $\sigma\gamma_A$ equal to zero is only slightly higher than the minimum ΔV_D. The associated orbiter lead angles are very close to the values for the minimum ΔV_D. The use of this strategy allows lower nominal γ_A than those shown in Fig. 8, but has the same problem as strategy (1) at the higher β.

Minimum Lander Antenna Aspect Angle (#3). The relay communication link between the lander and orbiting spacecraft during the entry phase is shown in Fig. 15. The boresight of the lander antenna is taken to be along the longitudinal axis. At entry the lander is in a zero angle of attack orientation. A positive lander aspect angle, α_L, is measured counterclockwise from the boresight axis to the line of sight between the lander and orbiting spacecraft.

The maximum and minimum α_L during entry is shown as a function of λ in Fig. 16 for a β of -30 deg. Both a large and a small orbit are shown. A lead angle of about -12 deg centers the maximum and minimum variation about zero. The variation is between $\pm$ 25 deg and $\pm$ 40 deg depending on orbit size. The maximum positive α_L occurs at entry and the maximum negative α_L occurs at touchdown. The effect of β, in the range from 0 to 40 deg, is slight in determining the λ which centers the variation. The corresponding ΔV_D variation with β for a λ of -12 deg is very close to that given in Fig. 5 for a λ of -10 deg.

Minimum Communication Range (#4). The communication range variation with λ is shown in Fig. 16, again for a β of 30 deg. The variation with apoapsis altitude is slight. The lead angle which minimizes the communication range during entry is between -2 and +2 deg depending on h_p. Corresponding to these lead angles the maximum ρ_c is about 250 KM higher than periapsis altitude and occurs near touchdown. The variation of ΔV_D with β for this strategy can be seen from Fig. 5 where a λ of 0 deg is shown.

Minimum Communication Fading Margin Losses(#5). A multipath analysis was made on the relay link during entry. The worst fading margin during entry is shown as a function of lead angle in Fig. 17. To insure good system performance the lead angles should be limited to the range $\pm$ 10 deg

Selected Maneuver Strategy

The selected maneuver strategy restricts lead angles to the range 0 to -10 deg. The lead angle variation with β is shown as a function of orbit size in Fig. 18. At low β a λ of 0 deg is used and continued until the minimum ΔV_D is reached. The λ is then varied between 0 and -10 deg along the minimum ΔV_D curve and then kept constant at -10 deg. A nominal operating region for β has been selected as 10 to 40 deg. For periapsis altitudes above about 1500 KM the λ is always a constant, -10 deg. The ΔV_D variation with β is shown in Fig. 5.

POST LANDING COMMUNICATION LINK

Relay Link

The analysis of lander to orbiter communication link geometry is always a troublesome task. The use of highly elliptical orbits complicates the task even more. In an effort to gain better vision of the effects of targeting variations and uncertainties on the link geometry, a somewhat different approach to the analysis was devised to replace the classical technique of running hundreds of orbit/landing site combination time histories. The technique, to be described in a future paper, is summarized below.

As the spacecraft travels around its orbit, there is a period of time it can see the landing site latitude. During that period, the right ascension, α, of the visible landing site latitude can be defined. A representative contour is illustrated in Fig. 19 for a 1300 x 12,500 orbit, inclined 45 deg to the Martian equator, and landing site latitude of -37 deg. The link constraints imposed on this contour are a ground elevation mask of 34 deg and a maximum communication range of 5000 KM. Since this contour exists every orbit, it is only necessary to see if the lander right ascension places it within the contour on any given orbit. Since the lander right ascension increases linearly with time (i.e. planet rotation), its time history can be superimposed on the spacecraft time history (Fig. 19).

The starting point of the lander position line is a function of targeting parameter, β, and spacecraft lead angle at touchdown, λ_{TD}. The link time is simply the time interval when the lander position line lies within the spacecraft contour. The correctness of the technique has been verified with many time history computer runs.

Once the size of the spacecraft contours is established ($\Delta\alpha$), an analysis technique such as that illustrated in Fig. 20 is used. The spacecraft $\Delta\alpha$ band occurs every 360 deg. The existence of a link on any given orbit number and orbital period requires that the orbit number line lie within the band. Thus, as an example from Fig. 20, a link will exist after the first day on orbit No. 3 for orbits with periods between 4.6 and 8.1 hours. The actual time of the link can be determined from the α scale, interpreted as time, (i.e. 360 deg is 24.624 hours).

The range of $\Delta\alpha$ for orbits with inclinations between 30 to 50 deg and periapsis altitudes of 500 to 2500 KM and apoapsis altitudes of 10,000 to 20,000 KM is 135 to 185 deg. The minimum occurs for the 500 x 20,000 KM orbit, the maximum for the 2500 x 10,000 KM orbit. The $\Delta(\Delta\alpha)$ shift as a function of β (shown in Fig. 20) varies from approximately 25 to 60 deg for β from 10 to 40 deg for a 1500 x 15000 KM orbit. The variation is insensitive to apoapsis altitude and varies approximately +10 deg per 1000 KM change in periapsis altitude.

These characteristics have been investigated to establish the maximum orbital period for which a link is assured at least once a day. These results are relatively insensitive to β and indicate a maximum orbital period varying from 9.2 to 12.5 hours for $\Delta\alpha$ between 135 and 185 deg, respectively. The limits on orbit size and shape resulting from these characteristics are presented below.

Lander to Earth Direct Link

The direct link geometry is a function of landing site latitude and date. The elevation angle of the Earth is shown in Fig. 21 as a function of universal time for λ_L of -20 deg and -40 deg. The effect of date is shown. On February 2, 1974, the landing sites of -20° and -40° can view the Earth for about eight hours of the day, assuming a 34 deg ground mask. A later arrival date decreases the link time to about six hours.

If a direct link is desired immediately after touchdown, the elevation angle of the Earth at touchdown is of importance. Landing near the evening terminator results in low elevations, as seen in Fig. 11 less than 34 deg, and the Earth is soon below the horizon. Landing near the morning terminator results in higher elevation angles and the landing site is rotating toward the sub-Earth point.

ORBIT SELECTION CRITERIA

The groundwork has now been laid for a reasonable

selection of nominal orbits which considers all mission constraints.

The selection of minimum periapsis altitude is based on the desire for an initial post touchdown communication link with the orbiting spacecraft of 3.5 to 5.0 minutes. The restrictions on orbit periapsis altitude for different link times are shown in Fig. 22. For a given orbit a combination of high targeting parameter, β , and orbiter lead angle, λ , result in the worst case for initial post touchdown link time. A value of 40 deg for β and zero deg for λ are used for the worst case based on the selected deorbit strategy given above. The required h_p for the worst case and 5 minutes 11e between 1250 and 1400 KM for a 34 deg mask. The 3.5 minute limit requires a minimum h_p of about 800 KM for a 15 deg ground mask. Assuming a 3σ h_p of 500 KM after the last midcourse correction, the minimum nominal periapsis altitude would be 1300 KM. A nominal h_p of 1300 KM has been chosen. Five minutes post touchdown link time would be achieved for all cases except where the worst case β and λ were required and a 34 deg ground mask existed in the orbital plane. If the 3 σ dispersion on h_p occurred in the low direction (i.e. 800 KM), the 3.5 minute limit would be satisfied for a 15 deg ground mask in the orbital plane. It does not seem reasonable to simultaneously assume a 3σ h_p dispersion and maximum ground mask, but if this did occur a link time of approximately one minute still exists to verify landing.

The next selection to be made is the apoapsis altitude limits. Here the assumption is made that the selection of orbital period in the pre-flight sense must have sufficient range to allow landing at any longitude after a fixed number of days after encounter. Table II shows that the most adverse post-orbit insertion period error due to navigation uncertainty at the time of transmittal of the orbit insertion impulse and firing direction commands and misapplication of the orbit insertion maneuver is 2 hours (3σ). It is assumed that the actual orbital period will not be adequately known from Earth based tracking for at least 4 orbits, allowing a time phasing error of up to 8 hours before an accurate orbit trim maneuver can be made. The orbit trim maneuver must compensate for this error if the preselected landing site is to be acquired. The trade here is on the selection of orbit number for nominal deorbit. If this is low, say 6 or 7, the required correction must compensate for the time phasing error in very few orbits (2 to 3 in this case) requiring a large orbit trim maneuver. A later nominal deorbit number, say 15 or 16, allows a much smaller trim requirement, but can result in a growing time phasing error introduced by misapplication of the orbit trim maneuver. This error source would have to be compensated for with the deorbit maneuver by selection of the targeting parameter, β , if the preselected site is to be acquired. As discussed in the section on Orbit Deviation from the Nominal, the period error after orbit trim could be as high as .243 hours (3σ) if the total allocated 150 M/SEC is used. This results in a longitude phasing error of 3.54 deg (3σ) per orbit. Table II shows that the total 3σ error in the periapsis location is 6.0 deg after orbit insertion which must also be accounted for to hit a preselected sight. These two error sources combined result in a total error of about 31 deg (3σ) for deorbit on the 12th orbit. A targeting capability, $\triangle\beta$, of 31 deg is then required. The results of the analysis of trading off orbit number show that deorbit on the fourth day, on either the 12th or 13th orbit (depending upon the desired longitude), is reasonable. The required range of apoapsis altitudes as a function of periapsis altitude and orbit number to allow landing at any longitude during the 4th day is shown in Fig. 23. To use the 12th or 13th orbit requires the range of nominal apoapsis altitudes to be between 11,500 KM and 13,500 KM for the nominal h_p of 1300 KM.

The 3σ range of possible orbits about the nominal selection after orbit insertion due to the combination of navigation uncertainty at the time of the last midcourse correction and orbit insertion errors (navigation and misapplication) is shown in Fig. 24. Also shown are the possible 3σ orbits after orbit trim. As discussed previously the orbit trim maneuver is made at periapsis and corrects to a new period (not the nominal) which cancels out the 8 hr (3σ)phasing error prior to orbit trim.

The restrictions on orbit size due to the targeting capability, $\triangle\beta$, required and due to design maximum $\triangle V_D$ can be seen from Fig. 10. Two boundaries are shown in Fig. 24 for a $\triangle\beta$ of 30 deg and a $\triangle V_D$ of 300 M/SEC. If it is decided after orbit insertion to land at any convenient location under the orbit within 15° to 30° from the terminator, a $\triangle\beta$ of from 24° to 28° might be required, depending on orbital inclination. There is again the 6° requirement due to error in the argument of periapsis, and the remainder is the $\triangle\beta$ variation needed to land between 15° and 30° of the terminator.

The nominal range of orbits is well above the orbit insertion constraint corresponding to a V_{HE} or 3.25 KM/SEC as discussed in the Orbit Insertion section. The constraint on orbit size due to the requirement for a post touchdown relay link every day as discussed in the Post Touchdown Relay Link section is seen to cut a small corner of the 3σ trimmed orbits. The 3σ trimmed orbits are well to the right of the 50-year lifetime boundary. A boundary for the initial post touchdown link is also shown. A boundary is shown for an early arrival date near the evening terminator with a i_{EQ} of -60° as discussed in Landing Site Selection. It must be recalled that the final orbit selection process is intimately dependent upon the mission constraints assumed.

CONCLUSIONS

1. Nominal h_p = 1300 KM
2. Nominal h_A between 11,500 KM and 13,500 KM depending on longitude of desired landing site
3. Deorbit during 4th day on 12th or 13th orbit depending on longitude of landing site
4. Targeting capability, $\Delta\beta$, of 30 deg ($10^\circ < \beta < 40^\circ$)
5. Maximum ΔV_D required is 300 M/SEC
6. Orbiter lead angles restricted to -10 deg to 0 deg range

SYMBOLS

α Right ascension of visible landing site for post landing link (Deg)

α_L Antenna aspect angle of the lander; measured positively from the boresight to the line of sight to the orbiting spacecraft (Deg)

β Targeting parameter; angle measured positively from the orbiter periapsis to the entry location opposite the orbital motion of the orbiting spacecraft (Deg)

γ_A Entry flight path angle measured from the local horizontal at entry (Deg)

$\delta_{HE_\oplus}$ Declination of the departure asymptote at Earth; measured with respect to the Earth's equator (Deg)

$\Delta\alpha$ Size of orbiting spacecraft contour for post land link (Deg)

$\Delta(\Delta\alpha)$ Location of initial post land link (Deg)

ΔV_D Impulsive velocity required for deorbit

$\Delta\beta$ Targeting capability (Deg)

$\Delta V_{O.I.}$ Impulsive velocity required for orbit insertion (KM/SEC)

$\Delta\phi$ Central angle traversed during entry (Deg)

Δ Angle of orbiter periapsis shift from the approach hyperbola periapsis; a positive shift places the orbiter periapsis further downrange (Deg)

θ_D True anomaly of the deorbit point (Deg)

θ_F Angle between periapsis of nominal orbit and periapsis of actual perturbed orbit (Deg)

λ Orbiter lead angle; central angle between lander and orbiter positions at the time of entry; positive if orbiter leads the lander (Deg)

λ_L Latitude of landing site (Deg)

λ_{TD} Orbiter lead angle at touchdown (Deg)

μ_{σ^*} Gravitational parameter of Mars ($42830.KM^3/SEC^2$)

ρ_c Communication distance between lander and orbiting spacecraft (KM)

σ_{γ_A} Standard deviation in entry flight path angle (Deg)

σ_ϕ Standard deviation in orientation angle (Deg)

σ_{DR} Standard deviation in downrange angle (Deg)

$\odot$ Astronomical symbol for the Sun

$\oplus$ Astronomical symbol for the Earth

σ^* Astronomical symbol for Mars

C_3 Twice the energy per unit mass required to transfer to Mars on a given launch and arrival date (KM^2/SEC^2)

h_p Periapsis altitude, point of closest approach of the orbiting spacecraft (KM)

h_A Apoapsis altitude, furtherest distance of the orbiting spacecraft (KM)

i_{EQ} Inclination of the orbiter's orbital plane at Mars with respect to the Martian equator (Deg)

R_{c_σ} Radius of Mars (3393 KM)

t/p Time, non-dimensionalized by orbital period

t_c Coast time (Hrs)

V_{HE} Hyperbolic excess velocity at Mars - the velocity of the planetary vehicle with respect to Mars upon entering the Martian sphere of influence (KM/SEC)

x, y, z Axis system used for the covariance matrix of position and velocity due to navigation uncertainties at the time of deorbit; z-axis is in the direction of the deorbit point; x-axis is in the orbital plane rotated 90 deg clockwise from z when looking down the angular momentum vector; y-axis is normal to the orbital plane and opposite the direction of the angular momentum vector

FIGURES

1. Mission Profile
2. Mars 1973-I Energy Contours
3. Orbit Insertion Impulse Capability
4. Deorbit Geometry
5. Deorbit Impulse Required
6. Entry Flight Path Angle Dispersion due to Pointing
7. Entry Flight Path Angle Dispersion due to Impulse
8. Entry Corridor
9. Deorbit Impulse: Effect of Entry Flight Path Angle
10. Range of Targeting Parameter
11. (a) Early Arrival Geometry

11. (b) Late Arrival Geometry
12. Required Periapsis Shift
13. Orbit Limits Imposed by Periapsis Shift Required
14. Occultation Constraint on Orbital Inclination
15. Relay Communication Link During Entry
16. Entry Communication Link Characteristics
17. Frequency-Shift Keying Fading Margin
18. Selected Deorbit Strategy
19. Longitude Coverage by the Orbiting Spacecraft
20. Link Dependence Upon Orbital Period
21. Direct Earth Link
22. Post Landing Initial Relay Link
23. Apoapsis Altitude Selection Criteria
24. Final Orbit Selection Limits

TABLES

I. Mission Constraints

II. Orbit Insertion Error Summary

III. Deorbit Error Summary

REFERENCE

JPL TR 32-820, "Geometric Aspects of Ground Station/Satellite Communications" by Roger D. Bourke, dated 15 October 1965.

ACKNOWLEDGMENT

This work was performed in part under Contract 952001 for the Jet Propulsion Laboratory, California Institute of Technology, as sponsored by the National Aeronautics and Space Administration under Contract NAS7-100.

The information contained herein in no way constitutes a final decision by NASA or JPL or any other Government agency relative to its use in a Voyager-type program.

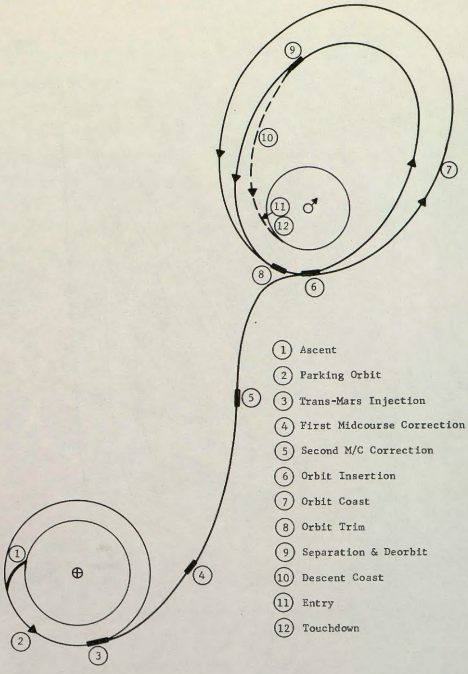

Fig. 1 Mission Profile

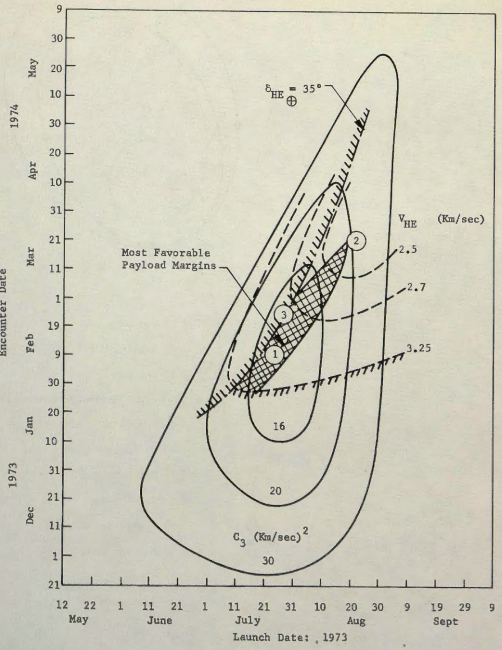

Fig. 2 Mars 1973-I Energy Contours

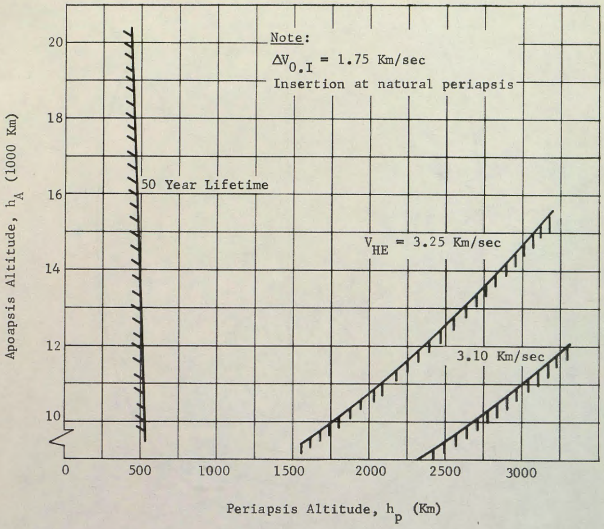

Fig. 3 Orbit Insertion Impulse Capability

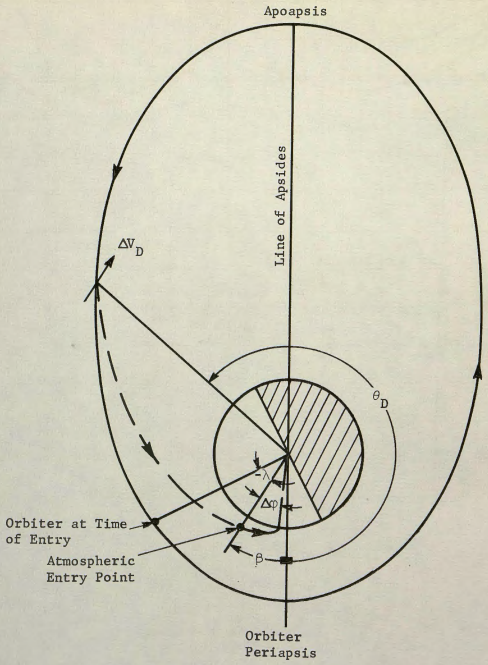

Fig. 4 Deorbit Geometry

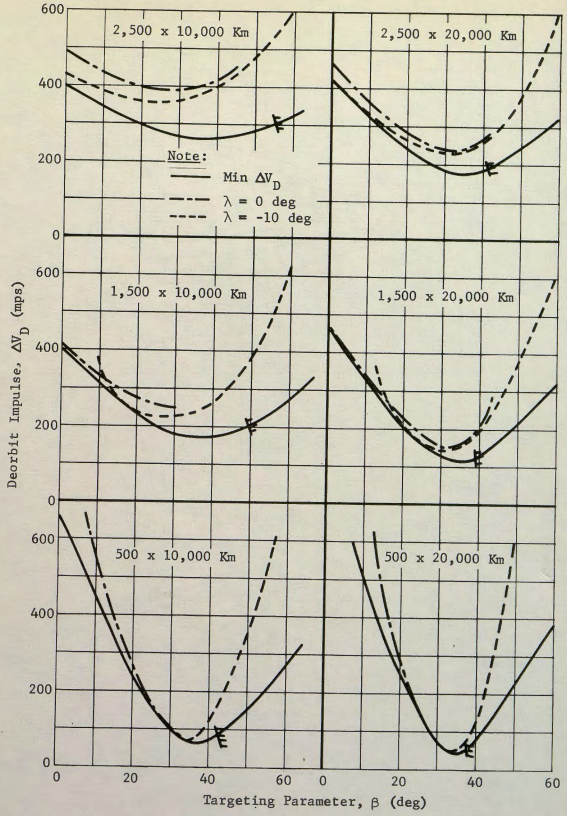

Fig. 5 Deorbit Impulse Required

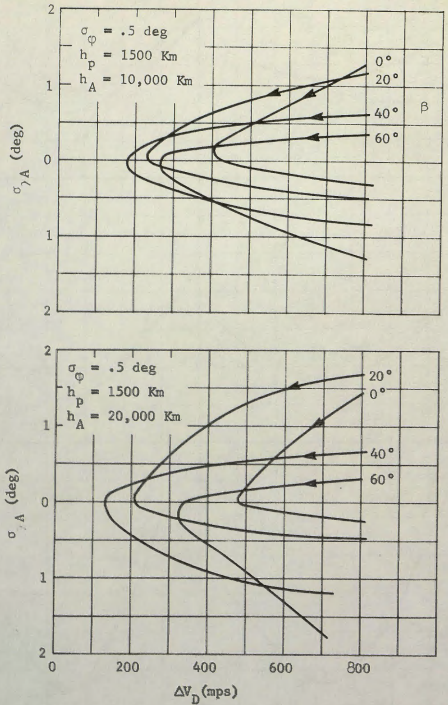

Fig. 6 γ_A Dispersion Due to Orientation

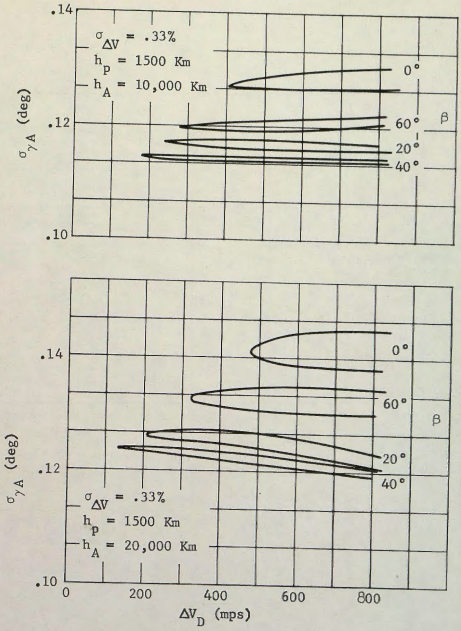

Fig. 7 γ_A Dispersion Due to Magnitude

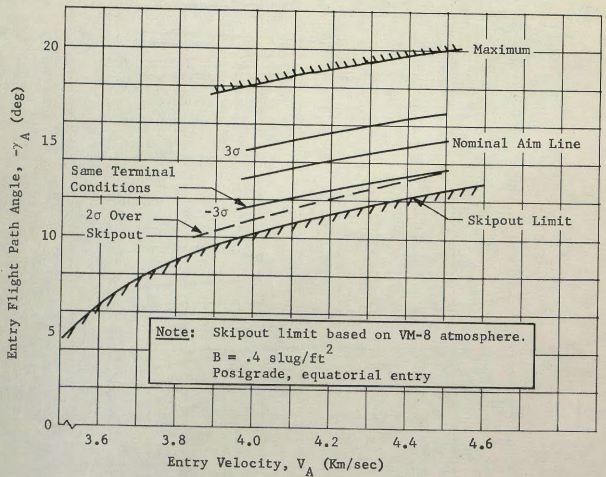

Fig. 8 Entry Corridor

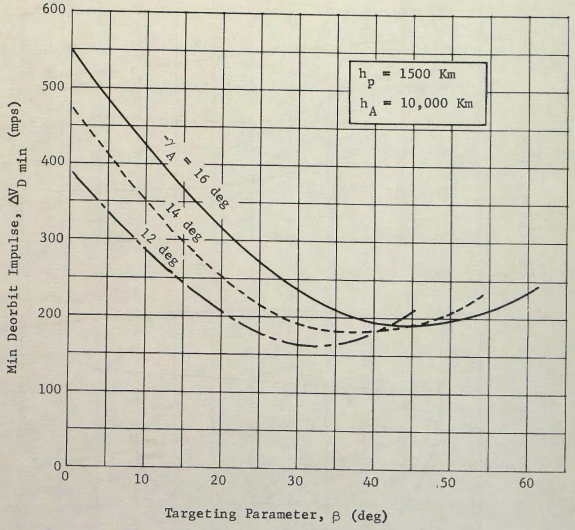

Fig. 9 Deorbit Impulse: Effect of Entry Flight Path Angle

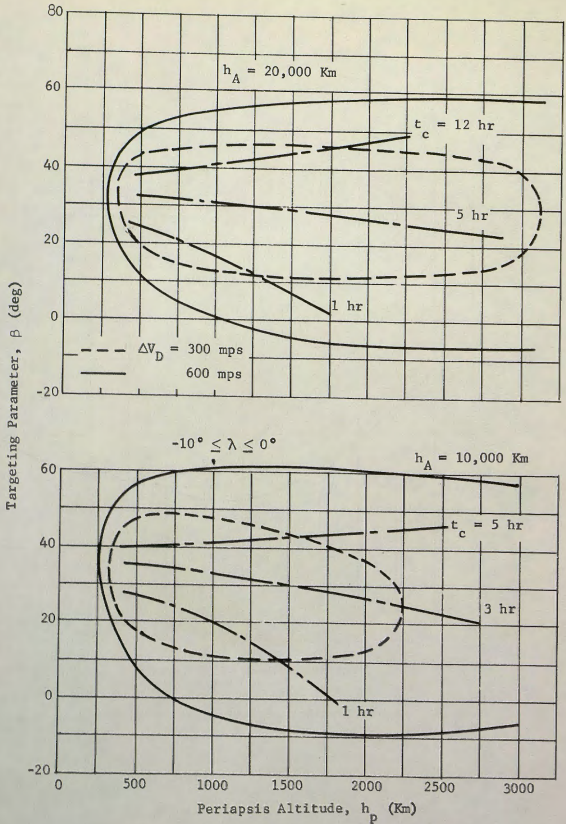

Fig. 10 Range of Targeting Parameter

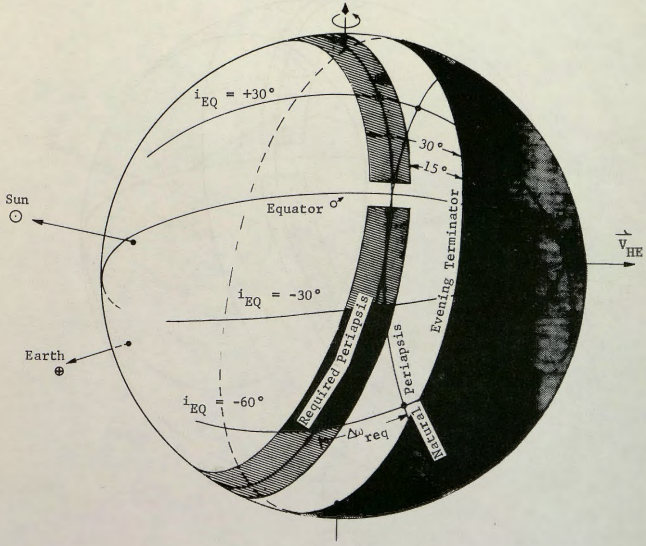

Fig. 11(a) Early Arrival Geometry

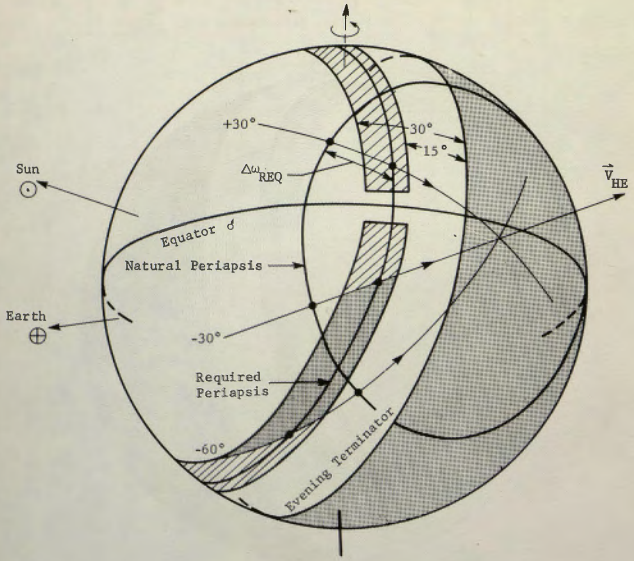

Fig. 11(b) Late Arrival Geometry

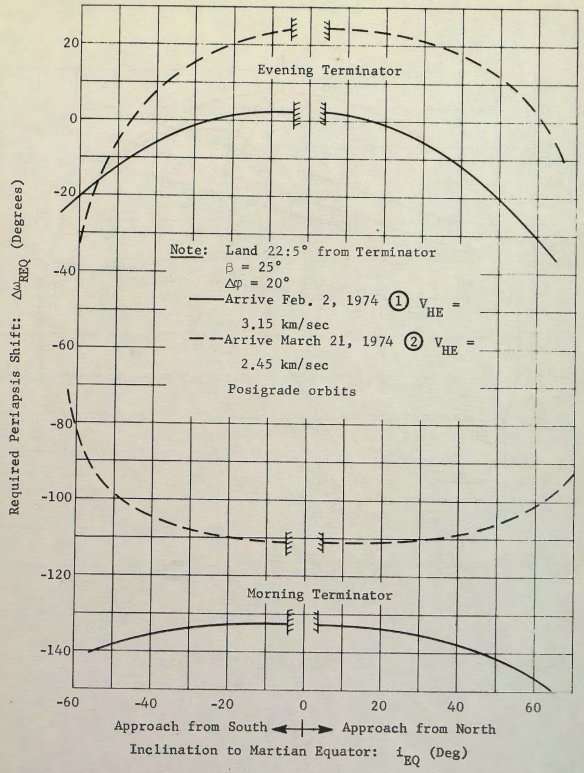

Fig. 12 Required Periapsis Shift

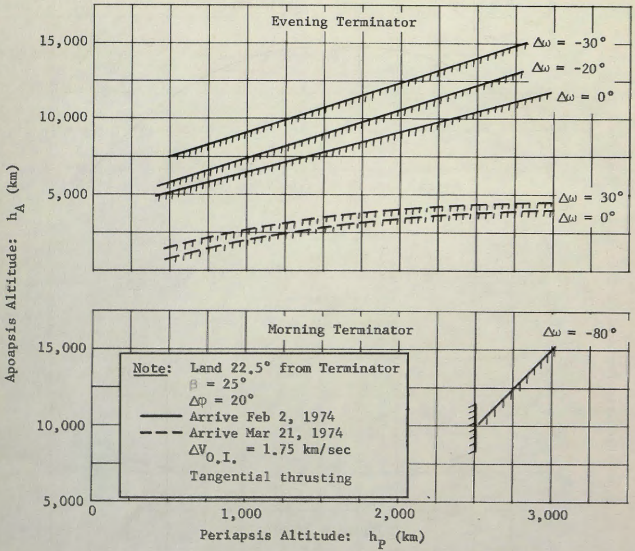

Fig. 13 Orbit Limits Imposed by $\Delta\omega_{REQ}$

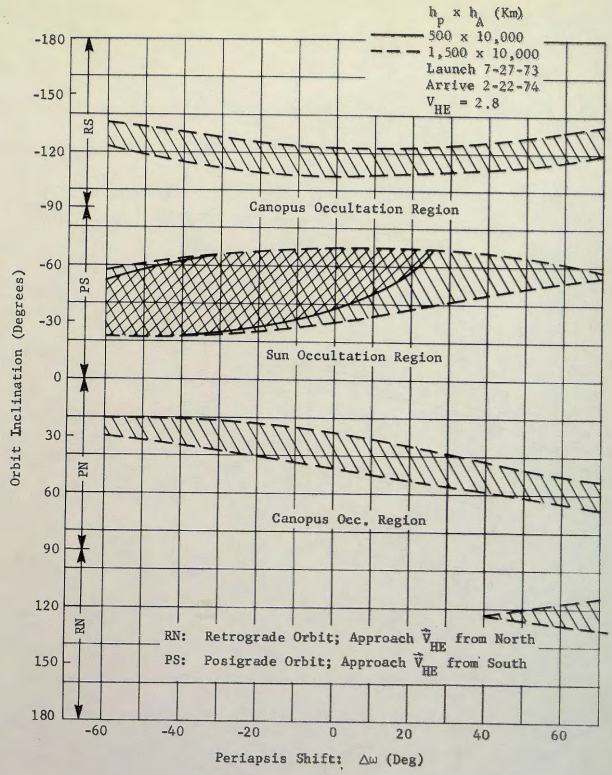

Fig. 14 Occultation Constraints on Orbit Inclinations

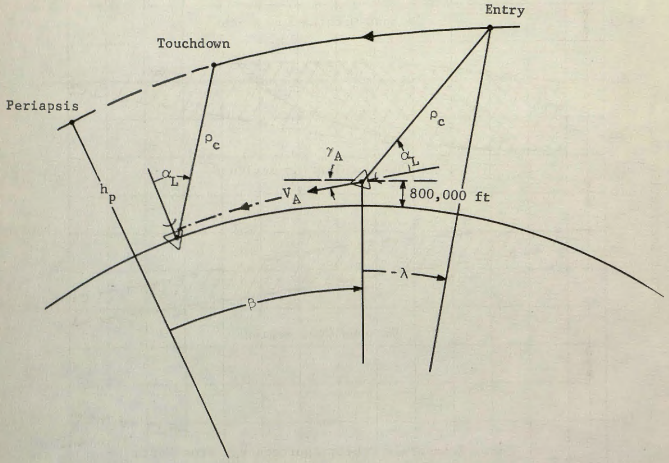

Fig. 15 Relay Communication Link during Entry

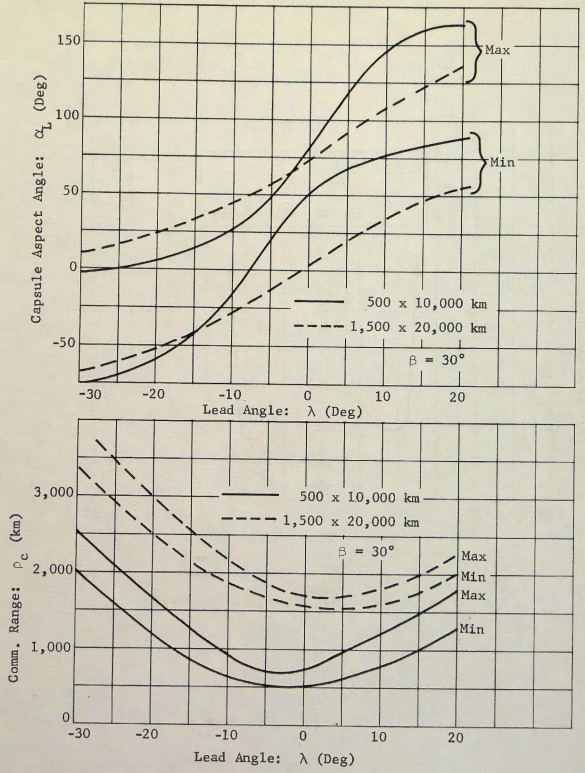

Fig. 16 Entry Communication Link Characteristics

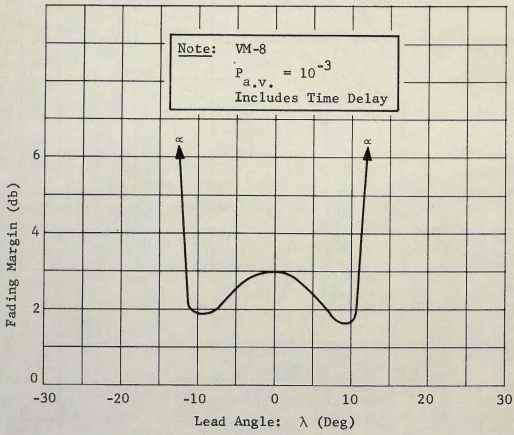

Fig. 17 Frequency-Shift Keying Fading Margin

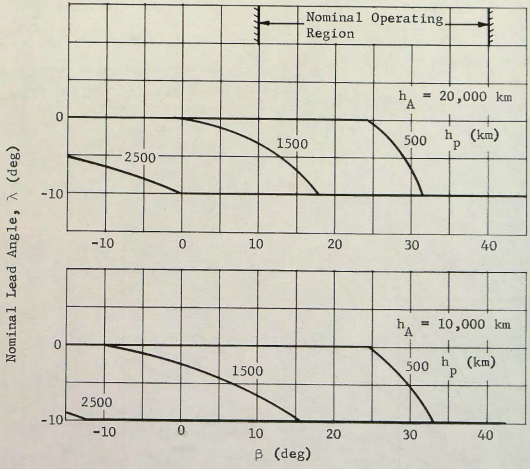

Fig. 18 Selected Deorbit Strategy

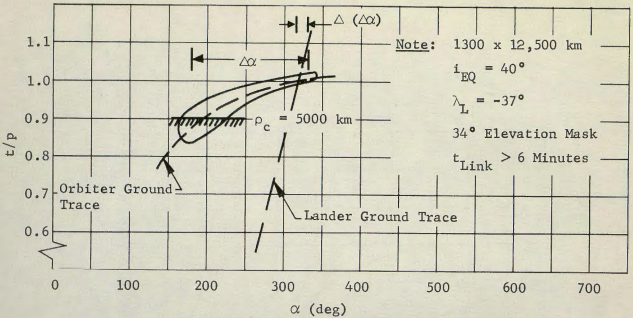

Fig. 19 Longitudinal Coverage by Orbiting Spacecraft

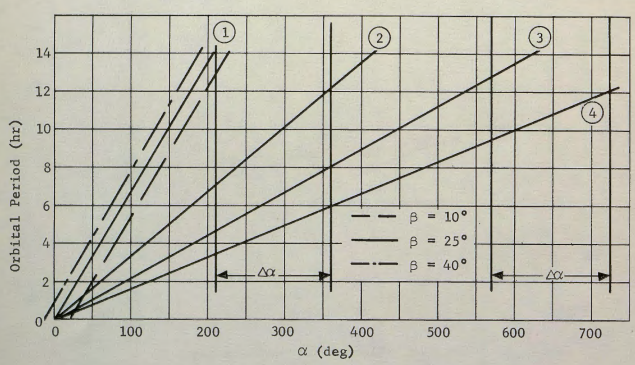

Fig. 20 Link Dependence upon Orbital Period

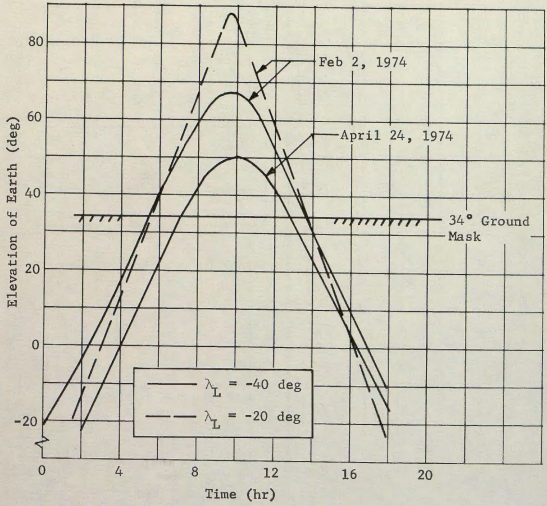

Fig. 21 Direct Earth Link

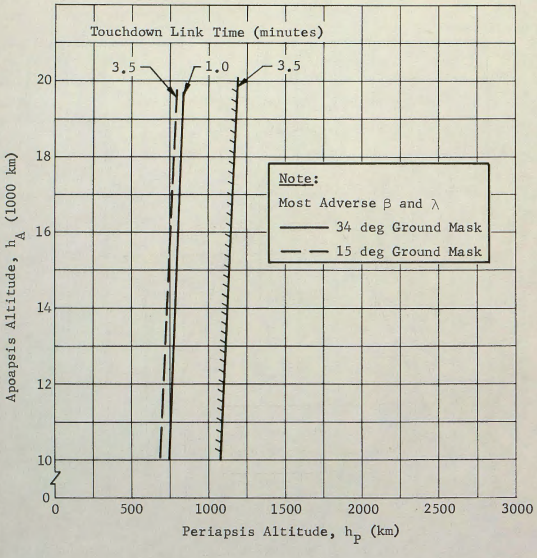

Fig. 22 Post Touchdown Initial Relay Link

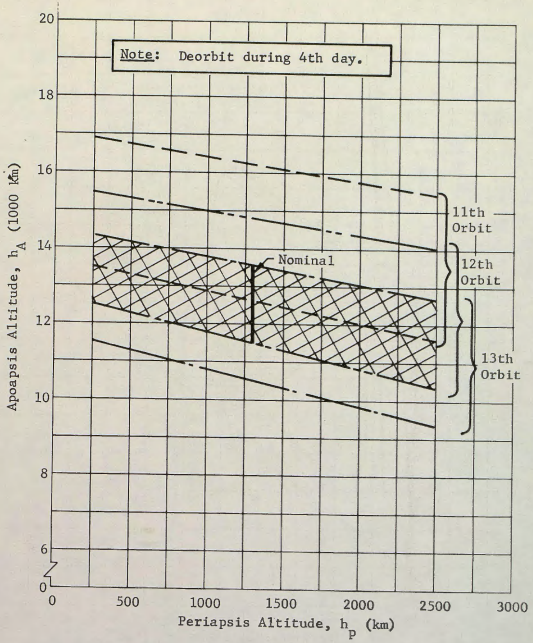

Fig. 23 Apoapsis Altitude Selection Criteria

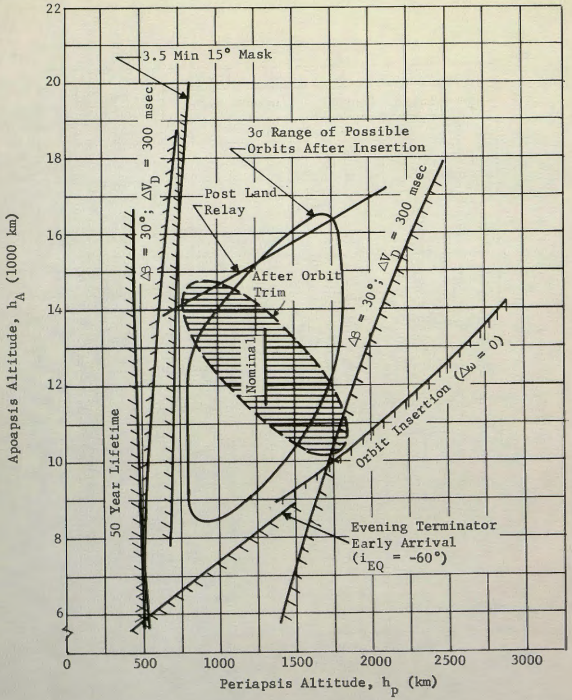

Fig. 24 Orbit Selection Limits